Review Article

Probing LHC halo dynamics using collimator loss rates at 6.5 TeV

A. Gorzawski,[1,2,*,†] R. B. Appleby,[3,4] M. Giovannozzi,[1] A. Mereghetti,[1] D. Mirarchi,[1] S. Redaelli,[1] B. Salvachua,[1] G. Stancari,[5] G. Valentino,[2] and J. F. Wagner[1,6]

[1]*CERN, Beams Department, Esplanade des Particules 1, 1211 Geneva, Switzerland*
[2]*University of Malta, Msida, MSD 2080 Malta*
[3]*The University of Manchester, Manchester M13 9PL, United Kingdom*
[4]*The Cockcroft Institute, Warrington WA4 4AD, United Kingdom*
[5]*Fermi National Accelerator Laboratory, Batavia, Illinois 60510, USA*
[6]*Goethe-Universität Frankfurt am Main, 60323 Frankfurt, Germany*

(Received 11 March 2020; accepted 8 April 2020; published 27 April 2020)

Halo diffusion measurements at the CERN Large Hadron Collider (LHC) were conducted with beams for physics at 6.5 TeV by means of collimator scans, carried out between 2016 and 2018. From the time evolution of the beam losses recorded during a collimator scan, in which collimator jaws are moved in steps toward the beam core cutting beam tails, one can extract information on the halo diffusion and its population as a function of the transverse amplitude. In this paper, results of the first scans performed at different beam intensities for both planes and both beams using the primary collimators of the betatron-cleaning system are presented. The scans were performed with squeezed optics and colliding beams after a few hours of regular physics production, during so-called end-of-fill measurements. Beam losses are measured with ionization chambers close to the collimators, which enable 1 and 100 Hz acquisitions, as well as diamond beam loss monitors, which enable turn-by-turn and bunch-by-bunch acquisitions. Parametric fits of a diffusion model are applied to the time profile of losses, for both total and individual bunch intensity. The analysis of the measurements performed in various conditions was used to estimate the diffusion coefficient as a function of the transverse amplitude and the population of LHC beam tails.

DOI: 10.1103/PhysRevAccelBeams.23.044802

I. INTRODUCTION

Inevitable particle losses occur at each stage of the operation of particle accelerators. These losses are due to the dynamics of the particles in an accelerator that usually is quite complex. Various mechanisms such as lattice nonlinearities, beam-gas interaction, and beam-beam effects may contribute to the topology of the particles' phase space. In addition, noise sources like ground motion and ripples in the radio-frequency devices or the magnet power supplies can interplay with the particle motion, resulting in diffusive dynamics. Excessive diffusion may result in an increased rate of the halo repopulation, emittance growth, and, eventually, for the high-amplitude particles, an increase of beam losses. These aspects are particularly important for high-intensity superconducting accelerators where beam losses put at risk the operation of superconducting magnets and can damage accelerator components.

The CERN Large Hadron Collider (LHC) consists of eight arcs and eight insertion regions (IRs), four of which house experiment detectors [1]. The total stored energy in the LHC 6.5 TeV beams exceeds 300 MJ. A multistage collimation system was installed to provide beam cleaning and passive protection against beam losses [2]. Betatron halo cleaning is concentrated in IR7, while off-momentum cleaning is concentrated in IR3. Local triplet magnet protection and physics debris collimation cleaning are located at the colliding IRs (IR1, IR2, IR5, and IR8).

The LHC collimators are kept at tight gaps throughout the operational cycle, as small as 1 mm at top energy for the collimator jaws closest to the beam, in order to ensure adequate machine protection and cleaning against beam losses. This system protects the LHC aperture and, in particular, the superconducting magnets against quenches (sudden transitions from the superconducting to the normal-conducting state), by concentrating beam losses in warm areas. Collimators can serve as powerful diagnostics instruments, e.g., to probe the beam tails, through transverse position scans [3]. Presently, this is the only method to measure with sufficient resolution the beam tails above three sigmas of the high-intensity LHC beams.

*arek.gorzawski@cern.ch
†Also at The University of Manchester.

The High-Luminosity LHC (HL-LHC) [4] will start operating in 2027 and will push forward the luminosity frontier, increasing by about a factor of 10 the LHC integrated luminosity. It is planned to operate the HL-LHC with higher-brightness beams [5] that carry about twice the LHC bunch charge with an emittance about 1.5 times smaller than the LHC design values, similar to what was achieved in LHC run 2. Halo losses with these beams pose concerns for the operation of the HL-LHC, in particular, in light of measurements carried out at the LHC that indicate significantly overpopulated beam tails [6]. While a direct extrapolation to the HL-LHC parameters is difficult, it is important to measure beam tails and their diffusion at the LHC in conditions as close as possible to those that will be deployed after the upgrade. Establishing empirical diffusion models can also improve modeling of loss and collimation mechanisms at the HL-LHC.

The first set of diffusion measurements at the LHC was taken at 4 TeV in 2012 [7,8] when detailed procedures were established and a diffusion model was first applied to the LHC data. The measurements were repeated in LHC run 2, between 2015 and 2018, for the first time at 6.5 TeV [6], in conditions that are more representative of the HL-LHC operational conditions, in terms of both beam energy and machine configuration [9]. In particular, probing higher bunch intensities of 1.7×10^{11} protons per bunch could be done for a case during a dedicated machine development study.

An improvement with respect to the LHC 2012 measurements [8] and previous ones carried out at the Tevatron at Fermilab [10] is that faster beam loss measurements were available for the 6.5 TeV experiments. In addition to 1 and 100 Hz data acquisitions, run 2 measurements profited from the bunch-by-bunch loss measurements from new diamond detectors. These devices were installed in several locations around the LHC ring during long shutdown 1 (2013–2015) and, specifically, in the betatron-cleaning insertion in the LHC [11] next to the primary collimators that were used during the measurements described in this paper.

The plan of the paper is as follows. In Sec. II, we recall the theoretical model used for the diffusion analysis, and in Sec. III, we present the experiment methodology, the machine configurations considered, and the beam instrumentation used. The 6.5 TeV measurement results are presented in Sec. IV, including the estimated diffusion coefficient and the halo-population reconstruction. This analysis includes bunch-by-bunch measurements performed in 2017 and 2018 that are used to characterize the differences between "bunch families" within the LHC bunch train structure. Finally, in Sec. V, some conclusions are drawn and an outlook for future measurements is discussed. In the Appendix, we collect a preview of the spectral analysis of the losses recorded during the experiments. That analysis was completed during the studies but it is beyond the scope of this paper.

II. DIFFUSION MODEL

A. Description

The diffusion model used to interpret the measured data for collimator scans is presented in detail in Refs. [8,12]. The model describes the time evolution of losses before, during, and after collimator steps (inward or outward, later denoted by the subscripts I and O, respectively).

Let $f(J,t)$ be the phase-space density described by the diffusion equation $\partial_t f = \partial_J(D\partial_J f)$. J is the Hamiltonian action and D the diffusion coefficient. The particle flux (ϕ) at a given location $J = J'$ is $\phi = -D \times [\partial_J f]_{J=J_c}$. The action J_c (during the collimator step) is computed at the location of the collimator as $\frac{x^2}{2\beta}$, where β is the beta function and x the average collimator jaw distance from the beam orbit. If D is constant, the local diffusion equation becomes $\partial_t f = D\partial_{JJ} f$. With these definitions, the particle loss rate at the collimator is equal to the flux at that location:

$$L = -D \times [\partial_J f]_{J=J_c}. \tag{1}$$

The loss rate evolution measured by the beam loss monitors can be expressed in terms of the particle loss rate L, a calibration constant k, and a background term B as $S = kL + B$. The loss evolution in time is proportional to the gradient of the distribution function at the collimator. The function f is computed at each value of J where collimator steps are performed, J_{ci}, as

$$\partial_J f_I(J_c,t) = \underbrace{-A_i + (2A_i - A_c)P\left(\frac{-J_c}{w}\right) - \frac{2A_i(J_{ci}-J_c)}{\sqrt{2\pi}w}}_{\text{loss offset, start, and end point}} + \underbrace{\frac{2(A_iJ_{ci}-A_cJ_c)}{\sqrt{2\pi}w}}_{\text{loss decay}} \underbrace{\exp\left\{-\frac{1}{2}\left(\frac{J_c}{w}\right)^2\right\}}_{\text{loss rise}}, \tag{2}$$

$$\partial_J f_O(J_c,t) = \underbrace{-A_iP\left(\frac{(J_{ci}-J_c)}{w}\right) + (2A_i - A_c)P\left(\frac{-J_c}{w}\right)}_{\text{loss offset, start, and end point}} + \underbrace{\frac{2(A_iJ_{ci}-A_cJ_c)}{\sqrt{2\pi}w}}_{\text{loss decay}} \underbrace{\exp\left\{-\frac{1}{2}\left(\frac{J_c}{w}\right)^2\right\}}_{\text{loss rise}}, \tag{3}$$

where A_i and A_c are the slopes of the distribution function before and after the step, respectively. $P(x)$ is a cumulative Gaussian distribution function. The parameter w is defined as $w \equiv \sqrt{2Dt}$. It exposes explicitly the dependence of losses on the inverse square root of time, as is typical for diffusion processes.

From the diffusion coefficient at a certain action value J_i, one can approximately compute the escape time of a particle, defined as the time that the particle would take

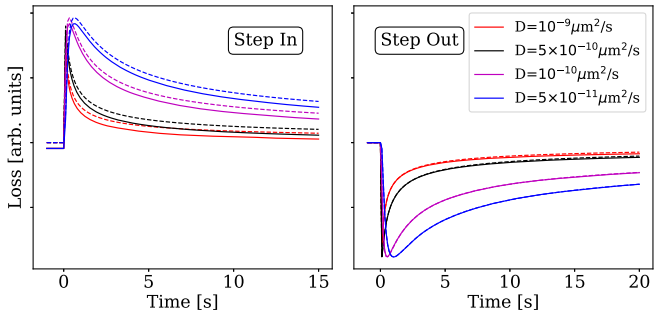

FIG. 1. Loss evolution for different values of the diffusion coefficient following Eqs. (2) and (3). Solid and dashed lines represent two approaches to the model simplification, described later in Sec. II.

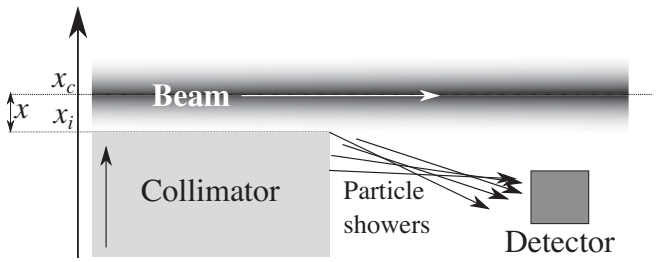

FIG. 2. Illustrative scheme of the collimator scraping apparatus for probing beam tails: one collimator jaw is moved into the beam, while the induced beam losses are measured locally by means of beam loss monitors.

to reach the collimator jaw at a larger action $J_f > J_i$, as $t_{\text{escape}} \simeq \frac{(\Delta J)^2}{D}$, where $\Delta J \equiv J_i - J_f$. Typically, J_f is taken as the operational value of the collimator gap that defines the smallest machine aperture, i.e., the initial aperture of the primary collimators. In this case, t_{escape} gives the time for a particle to reach the collimator in the approximated assumption that its transverse diffusion remains constant at its initial value $D(J_i)$.

B. Parametric fits

Figure 1 shows the time evolution of losses as predicted by the model for in and out steps, Eqs. (2) and (3), visualized for different diffusion coefficient values for the same jaw movement.

In the model, we identified three main components [explicitly labeled in Eqs. (2) and (3)] that describe the loss evolution during (i) the initial-state loss before the scan, referred to as the *loss offset*;(ii) the evolution of the loss during the step, referred to as the *loss rise*; (iii) the evolution of the loss decay as the particle distribution changes, called *loss decay*. In the majority of the analyzed cases, we used the model as described above, referred to as a *full model*. However, for testing some cases related to the data quality and for reasons described later (see Sec. III E), we simplified the model, by neglecting the first term describing the evolution of the initial-state loss, resulting in the *simplified model* denoted with S with the loss evolution described as

$$\partial_J f_{SI/SO}(J_c, t) = \underbrace{\frac{2(A_i J_{ci} - A_c J_c)}{\sqrt{2\pi} w}}_{\text{loss decay}} \underbrace{\exp\left\{-\frac{1}{2}\left(\frac{J_c}{w}\right)^2\right\}}_{\text{loss rise}}. \quad (4)$$

III. EXPERIMENT METHODS

A. Experimental setup and procedure

The experiments were carried out through collimator scans, where one jaw of the IR7 primary collimators (called TCPs) is moved into the beam in small steps while local losses are recorded, as schematically shown in Fig. 2. Robust primary collimators made of a fiber-reinforced carbon composite were used. The rest of the LHC collimators were kept at their nominal positions in order to ensure that the machine remained protected during the test. The scans start after a beam-based alignment [13] of the collimator to determine precisely its center, x_c, thus allowing one to compute the jaw position at each step x_i, in sigma units as $(x_i - x_c)/\sigma_N$. Here, $\sigma_N = \sqrt{\frac{\beta \varepsilon_N}{\beta_r \gamma_r}}$ is the nominal betatron beam size, for the nominal emittance $\varepsilon_N = 3.5$ μm, where β_r and γ_r are the relativistic factors and β is the betatron function. Throughout this paper, we always refer to the normalized emittance.

For tests at high stored beam energy, the scraping range spans from the starting TCP operational positions to a minimum distance from the beam orbit that was typically limited by the amount of losses generated versus the operational settings of beam loss monitor dump thresholds. Depending on the total beam current, values down to about $2.2\sigma_N$ could be reached.

The scraping was carried out with a single jaw. The centering and the scraping procedure were repeated for both planes and beams, in different conditions (e.g., with colliding or noncolliding beams). The scraping was typically performed with inward steps of 5 μm and outward steps of 20 μm. The reason for larger steps outward was to have a sufficiently high step down in the initial loss signal. Some examples are discussed in more detail in Sec. III E.

B. Machine configuration and beam parameters

Measurements were carried out in various campaigns from 2016 to 2018, at 6.5 TeV. Relevant machine configurations and beam parameters are listed in Table I. We recall the amplitude function β^* at the high-luminosity experiments in interaction points 1 and 5. Different optics were used in different years. In particular, since 2017, the so-called achromatic telescopic squeeze (ATS) optics was used. It introduced optics variations in the arcs to reduce the β^* at the collision points [14].

TABLE I. Main ring parameters for the LHC and the beam usual during run 2 for the end-of-fill scraping tests.

Parameter	2016	2017	2018
Beam energy [TeV]	6.5	6.5	6.5
Bunch spacing [ns]	25	25	25
Collimator half gap at 6.5 TeV [σ_N]	5.5	5	5
β^* (IP1/5) [m]	0.4	0.4	0.25
Optics	Nominal	ATS	ATS
Crossing angle [μrad]	185	145	145
Initial bunch intensity [10^{11} ppb]	1.1	1.2[a]	1.2[a]
Beam emittance [μm]	2.5	2.0	2.0
Beam energy before scraping [MJ]	170	260	260

[a]Bunch intensities up to 1.7×10^{11} p could be obtained during machine studies.

TABLE II. Lattice β functions and 6.5 TeV beam sizes in the collimation plane, with the nominal emittance of $\varepsilon_N = 3.5$ μm (σ_N) and the measured emittance of $\varepsilon = 2.0$ μm (σ), at the primary collimators in IR7. Values listed are for beam 1.

Collimator	β [m]	σ_N [μm]	σ [μm]
TCP.D6L7 (vertical)	78.3	198	150
TCP.C6L7 (horizontal)	150.44	275	208

Table II lists σ_N at the horizontal and vertical collimators and the respective β-function values. The nominal emittance $\varepsilon_N = 3.5$ μm as well as the typical average beam emittance recorded in the measurements, $\varepsilon = 2.0$ μm, are used to compute beam size values. The lattice functions in the collimation insertions were kept constant by design in the machine optics schemes used in 2016–2018. The values listed in the table are for beam 1. The design values for beam 2 are less than 1% different. This difference is small compared to the minimum lattice function uncertainty of 2% from β-beating measurements in the LHC [15].

The list of measurement campaigns is given in Table III together with some information specific to the fills: list of beams or planes that were measured, initial intensities, scraping ranges, and intensity lost during scraping.

Except for the case of fill 7392, when a dedicated fill was devoted to these measurements, the collimator scans were performed in standard physics fills as an "end of fill." After several hours of data taking in the experiments, following the standard LHC cycle, the machine was put in a safe mode with detectors off and the scraping was performed before dumping the beams for a fresh fill. Only acquisitions with colliding beams were possible in this case. The case of fill 7392 provided the unique opportunity to probe diffusion before and after putting beams in collisions.

C. Beam loss measurement

The data analysis relies primarily on the measurement of electromagnetic and hadronic showers induced when the collimator jaws intercept the beam particles. The standard beam loss monitoring (BLM) system of the LHC uses about 4000 ionization chambers (IC-BLMs) distributed around the rings. The charges collected by the ionization chamber from the secondary particles created from lost protons are read out using charge to frequency conversion with a dynamic range of 10^8, corresponding to currents from 10 pA to 1 mA. The measurement is provided in Gy/s in 12 different moving windows known as "running sums", ranging from 40 to 83.9 μs. This allows the configuration of unique beam extraction thresholds as a function of the duration of the beam loss. Different beam abort thresholds as a function of the beam energy are also used [16].

During the experiment, we used the monitors located in the vicinity of the primary collimators, specifically, (i) the

TABLE III. Summary of the measurements performed at 6.5 TeV, where n is the total number of bunches, I_{st} is the total intensity at the start of the scraping, and I_s is the total intensity lost during scraping (including luminosity burnoff). σ_s is the scraped range in measured beam sigma starting from 5σ.

			Beam 1			Beam 2			Scans performed	
Fill	Date	n	I_{st} [10^{13} p]	I_s [10^{13} p] (% of I_{st})	σ_s	I_{st} [10^{13} p]	I_s [10^{13} p] (% of I_{st})	σ_s	Beam	Plane
4910	2016-05-11	313	2.7	0.26 (6%)	1.5	2.8	0.26 (5%)	1.5	B1/B2	H/V
5105	2016-07-20	2076	15.0	1.10 (7%)	1.5	15.0	0.91 (6%)	1.5	B1/B2	H/V
5834	2017-06-15	900	8.8	0.59 (7%)	1.5	9.0	0.33 (4%)	1.5	B1/B2	H/V
5848	2017-06-20	1741	12.0	1.20 (10%)	1.5	13.0	0.49 (4%)	1.5	B1/B2	H
5849	2017-06-21	2029	13.0	0.98 (8%)	1.5	13.0	0.52 (4%)	1.5	B1H B2V	
6052	2017-08-06	2550	19.0	2.30 (12%)	1.2	21.0	2.30 (11%)	1.3	B1/B2	H/V
6194	2017-09-13	224	2.7	1.10 (40%)	1.8	2.7	1.02 (36%)	1.9	B1/B2	H/V
7221	2018-09-26	2550	12.0	0.65 (5%)	1.2	15.1	0.34 (2%)	1.2	B1/B2	V
7264	2018-10-07	2550	13.0	0.82 (6%)	1.3	14.2	0.75 (5%)	1.4	B1/B2	H/V
7392	2018-10-30	300	2.1	0.23 (9%)	1.2	2.4	0.28 (10%)	1.2	B1/B2	H/V
7392[a]	2018-10-30	300	2.8	0.21 (10%)	1.2	3.1	0.26 (11%)	1.2	B1/B2	H/V

[a]Scraping done with unsqueezed, noncolliding beams.

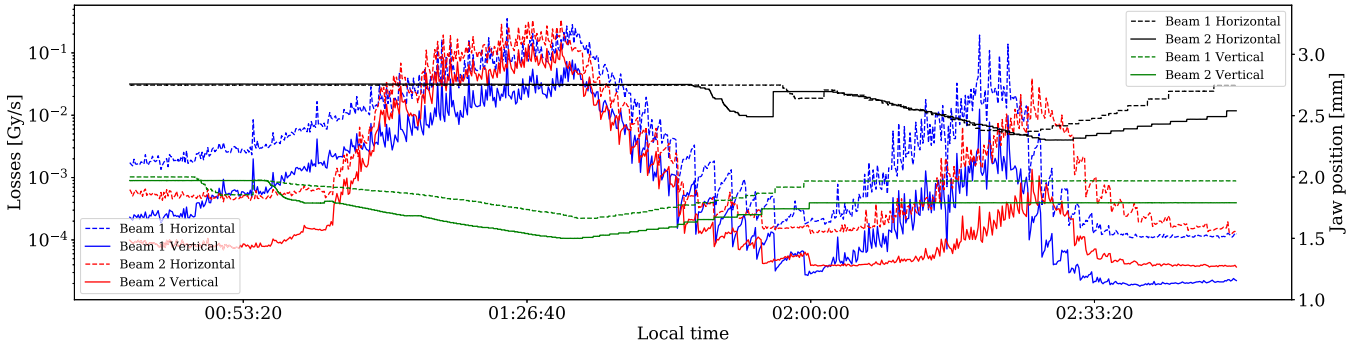

FIG. 3. Beam losses from the IC-BLM monitor. Beam 1 and beam 2 are shown in blue and red, respectively, and jaw positions during fill 6052 reported in Table III. Scraping is first performed on the vertical plane of the two beams at the same time; afterward, scraping is performed on the horizontal plane.

measured integrated losses published at 1 Hz as well as (ii) a special fast acquisition developed for collimator alignment purposes, which enables 100 Hz acquisitions.

Some example datasets for this acquisition mode are discussed in the Appendix in the context of frequency analysis. Note that, in previous measurements, the fastest sampling rate available was limited to 12.5 Hz [17].

The loss monitoring system has been extended with a new setup based on diamond beam loss monitors (dBLMs) that provide losses at a sampling time of 1.6 ns, therefore enabling bunch-by-bunch measurements of the 25 ns trains at the LHC. The dBLMs are installed in various locations in the LHC tunnel, and we used one monitor per beam located downstream of the collimators used for the scans [11]. The detectors are based on polycrystalline diamonds with a size of 10 mm × 10 mm × 0.5 mm. Diamond is a semiconductor, and particles traversing the detector generate electrons and holes in pairs, which drift in the externally applied electric field and induce a current signal collected by a preamplifier. The detector is connected to an ac-dc splitter, where the ac part of the signal is amplified by a current amplifier [18].

The dBLM system provides a "histogram acquisition mode" (later referred to as *acquisition mode 1*) where the source signal is looped (by synchronization to the LHC turn time of ≈89 μs) and divided in 1.6 ns bins, with an individual counter. This provides histograms of integrated loss distribution that are used to identify single-bunch losses. The histogram update rate is 1 Hz. In addition, one can access "waveform acquisitions" (later referred to as *acquisition mode 2*) of the raw data, recorded on demand for a short buffer (typically ≈200 ms) with the 1.6 ns sampling. These parameters allow one to reconstruct bunch-by-bunch and turn-by-turn losses. The latter acquisition mode can be used, for instance, for detailed spectral analyses of the loss signals. Additional information about the measurement setup and the data acquisition system is available in Ref. [11] and in the Appendix.

Beam loss data from the IC-BLM have a typical background level at 6.5 TeV of 10^{-5} Gy/s for the 100 Hz acquisition. The signals recorded during TCP scans ranged from 10^{-4} to 1 Gy/s. The graph in Fig. 3 shows the loss evolution and the moving jaw position for fill 6052 in Table III as an example. The dBLM acquisition system was active for this measurement and enabled a recording of the bunch-by-bunch losses. The histogram signal in acquisition mode 1 recorded some hundreds of counts per second, to be compared to background levels of a few counts per second. Figure 4 shows the bunch-by-bunch data as recorded. For acquisition mode 2, the raw data induced typical voltage values of 100 mV for the high loss cases, for signals of about 10^{-1} Gy/s in the IC-BLM.

D. Other beam observables

Other beam observables were recorded during the experiments.

1. Beam intensity data

The fast beam current transformers (FBCTs) were used to record the beam intensity: bunch-by-bunch and total beam current are available, sampled at 1 Hz.

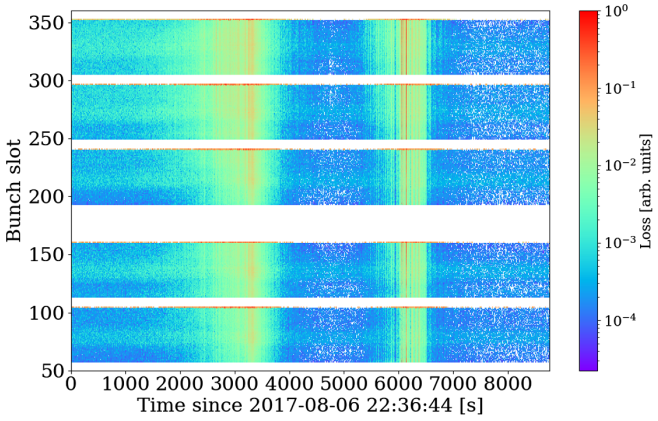

FIG. 4. Bunch-by-bunch loss from the dBLM monitor, recorded by acquisition mode 1 during the test in fill 6052 reported in Table III.

2. Bunch emittances

The synchrotron light monitor (BSRT, the Beam Synchrotron Radiation Telescope) provides continuous beam size measurements. The average values for each beam were logged every 3 s, and bunch-by-bunch measurements were also available. The emittance is then computed from the best estimate of the local optics [19]. Because of the large stored beam intensities, wire scanner measurements are forbidden, as the unavoidable beam losses would cause magnet quenches.

3. Collimator positions

The collimator jaw positions and gaps were logged at a rate of 1 Hz.

All the observables were logged with CERN Accelerator Logging System [20], except the dBLM, which at the time of the experiments had a customized data acquisition chain [11].

E. Data analysis methodology

The diffusion parameters were determined from the 100 Hz beam loss data, using the parametric fit described in Sec. II. With the full model functions (see Sec. II), the diffusion coefficient D was computed at each position explored by collimator steps. Automated tools were developed to find the moment of the scan step t_0 corresponding to the collimator jaw movement. Then, a 17-s-long time window was prepared between $t_s = t_0 - 2$ s and $t_e = t_0 + 15$ s for an inward step or a 27-s-long window with $t_e = t_0 + 25$ s for an outward step, to capture the decaying or increasing loss pattern. Once the beam losses and collimator positions were extracted, we applied the fit of the model for the decay obtained during an inward step [Eq. (2)] or an outward step [Eq. (3)] to get the diffusion parameter D for a given collimator action. We used a robust target objective function (as the sum of absolute deviations) as a figure of merit for the minimization problem. Examples of such fits are shown in Fig. 5. For the data coming from dBLM acquisition mode 1, we used the simplified model, because the data were collected at 1 Hz and the number of points available for the fit was too little to get reliable fit results.

The same analysis was applied to all the steps performed during the experiment. The results are discussed in Sec. IV B. We estimated the uncertainties on the model parameters by bootstrapping [21,22], with about 50 bootstrap resamples per collimator step. We always used 100 Hz loss data in order not to lose any loss pattern information. However, these data contained many oscillatory components revealed by frequency analysis [23] and briefly described in the Appendix. By using a robust target function (such as the sum of absolute deviations), the fit parameters are less sensitive to these oscillations and to other systematic effects. In addition, because the bootstrap method does not assume a model for the measurement uncertainties (such as Gaussian errors), the estimates of the parameter uncertainties are also robust.

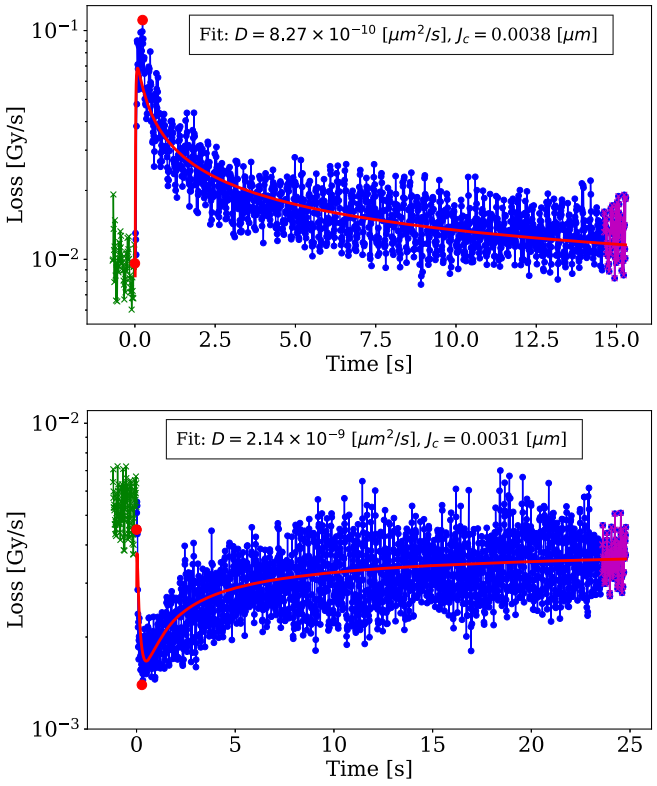

FIG. 5. Two examples for recorded data (blue) and fit results (red) for one of the inward steps by 5 μm (top) and outward step by 20 μm (bottom) step analysis. Highlighted green and magenta regions were used to establish the initial (A_i) and final (A_f) loss level. Examples from fill 6052 are reported in Table III.

The same procedure was applied to the dBLM acquisition mode 2 turn-by-turn data, available for one test in 2018 (fill 7392). For these cases, the end time of the data window (t_e) was defined by the buffer duration of about 0.25 s, and the result of such a fit is shown in Fig. 6.

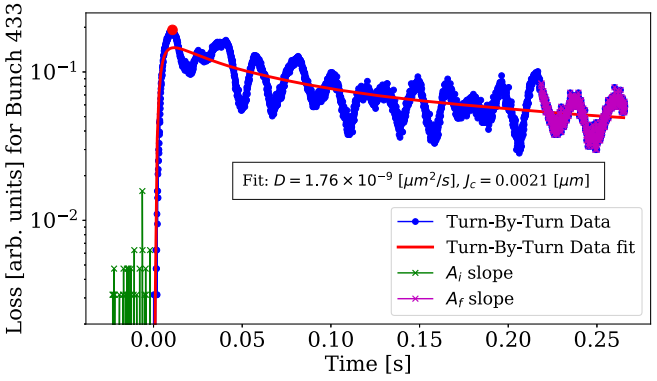

FIG. 6. An example of the fit result (red) for one bunch loss data (blue), recorded by dBLM acquisition mode 2 during fill 7392 reported in Table III. Highlighted green and magenta regions were used to establish the initial (A_i) and final (A_f) loss levels.

We are aware of certain limitations of the experimental method, in particular, regarding the length of the data acquisition during the scan step and, therefore, the loss decay level. Ideally, longer waiting times should be used to monitor the decay of loss spikes in order to ensure reaching steady conditions, but this would pose practical limitations on the scan ranges. Also, considering the experience in previous measurements and their results, e.g., at the LHC at 4 TeV [8] and the Tevatron [10], the waiting times were considered adequate for the approximate diffusion model used in this work. To test the sensitivity of the results to the duration of the waiting period, we tried intervals that ranged between 15 and 30 s and observed negligible differences.

F. Beam losses and tail population measurements

One can use the collimator scans also to estimate the beam halo population. To reconstruct the beam intensity profile as a function of the transverse amplitude, which we refer to as the *tail population* if the amplitude is larger than 3σ, one could, in principle, use the intensity loss from the FBCT signal at each collimator step. However, this instrument is not sufficiently precise to resolve losses in the case of small steps of collimator jaws.

The BLM system has instead a sufficient dynamic range to identify small tail losses. The BLM signal can be calibrated to obtain the number of lost protons per second from the measured dose in Gy/s through a proper conversion factor F in charges per Gy [24]. The integrated intensity loss due to the collimator step was computed as $\Delta I = F\Lambda$, where Λ is the integrated BLM signal in Gy. The step conversion factor is defined as $F = \Delta I_{\mathrm{tot}}/\Lambda_{\mathrm{tot}}$, where Λ_{tot} is the integrated step loss and ΔI_{tot} the absolute intensity lost recorded during the same step. An illustrative sketch introducing these quantities is shown in Fig. 7. In general, the conversion factor F depends on the position of the collimator jaw with respect to the beam. For this analysis, this dependence was negligible, and we used the same average conversion factor $F = 2.6 \times 10^{-13}$ Gy/p for all steps.

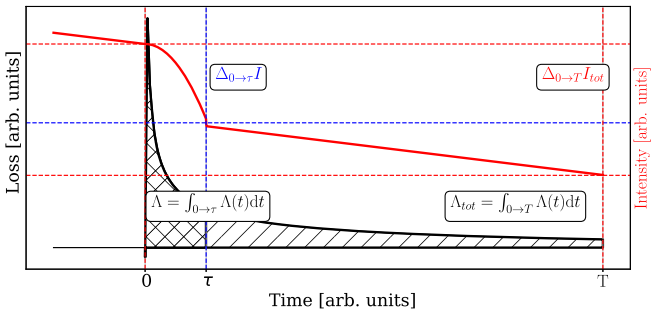

FIG. 7. Illustrative sketch for the algorithm used to compute the intensity lost (ΔI) due to the jaw movement ($0 \to \tau$) using the total loss (Λ_{tot}) decay phase (integral over $0 \to \mathrm{T}$).

IV. MEASUREMENT RESULTS

A. Halo population reconstruction

We consider fills 6052, 6194, and 7221 (Table III), because their beam intensities and emittances were the closest to the target HL-LHC values [25]. In these cases, a dedicated alignment before the scan was systematically executed, and the scan range was sufficiently extended, making these fills pertinent examples for our studies. Figure 8 presents the intensity loss and the collimator steps that were used for the reconstruction in fill 6052 along with markers that illustrate the time range used for halo reconstruction.

Figure 9 shows the reconstructed beam profile, obtained from the BLM signals using the conversion factor computed during the scans, i.e., 2.6×10^{-13} Gy/p. Gaussian profiles for the measured and nominal emittance ($\varepsilon_N = 3.5$ μm) are shown for comparison. One can notice an overpopulated tail, as separately reported from 2016 results [6] and in the remaining tests reported in this paper, with respect to the Gaussian distribution. For the case with the largest tail population (fill 6194), the integrated tail (3–5σ) population can reach up to 5% of the beam intensity, while the pure Gaussian distribution corresponding to the measured emittance would result in less than 1%. For the other scans (see Fig. 10), the estimated tail population was

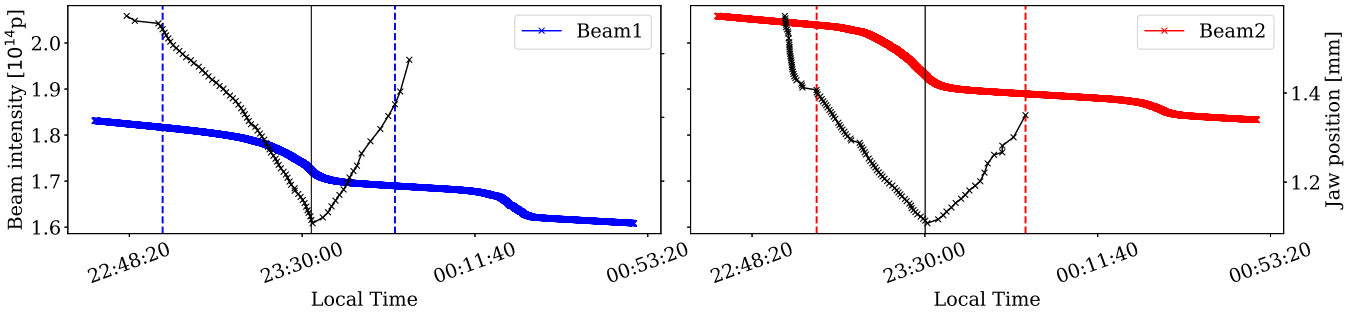

FIG. 8. Beam intensity and collimator jaw position during the scraping in fill 6052. The inward scraping was used to estimate the beam halo. The dashed lines represent the span of one experiment, for both inward and outward steps, whereas the solid black line marks the inversion of the collimator scan.

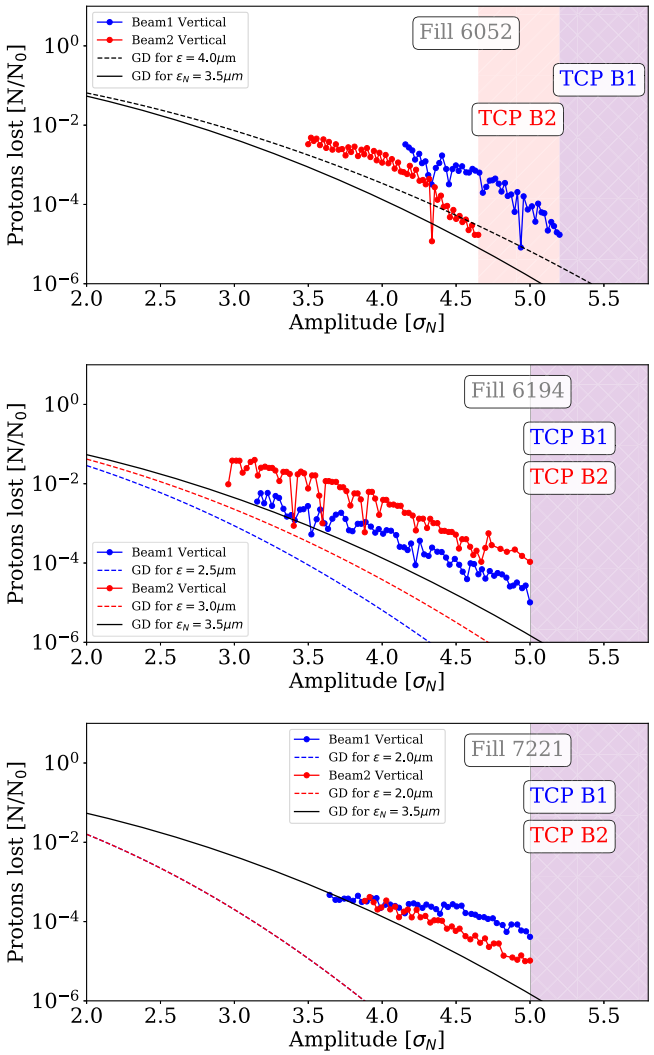

FIG. 9. Reconstructed beam profiles from the beam losses as a function of the jaw position during the selected scraping test (details in Table III), expressed in nominal beam size. All cases refer to the vertical plane, plotted along with Gaussian distributions (GDs) for different emittances. Fill 6052 (top), fill 6194 (middle), and fill 7221 (bottom). The TCP collimator jaw position at the end of the alignment, when the scan starts, is indicated by the color area on the right.

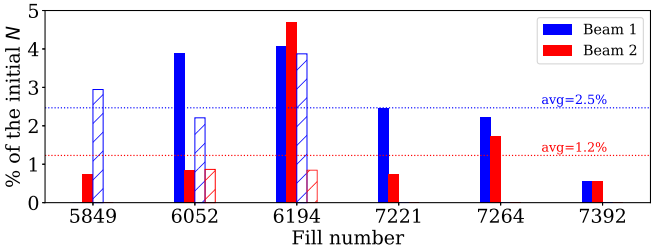

FIG. 10. Integrated intensity lost during the experiments. The data show the intensity reconstruction for the vertical (solid bar) and horizontal (hatched bar) plane for beam 1 (blue) and beam 2 (red).

below 2.5%. If this largest value was simply scaled with the total beam intensities to the HL-LHC conditions, this would correspond to about 36 MJ of energy stored in the beam tails [25]. Reaching higher values (beyond 5%) could be a potential problem for the cleaning system performance, but a detailed analysis of this subject is beyond the scope of this paper.

B. Diffusion coefficient

As described in Sec. II B, each collimator step and the time profile of losses that it generated were checked and modeled. A fraction of the collected data samples had to be rejected because of issues with the data quality (i.e., large oscillations or data dead time jeopardizing a good convergence of fits). The computed diffusion coefficients as a function of the transverse amplitude are shown in Fig. 11 for the available cases: horizontal and vertical for inward and outward steps, for both LHC beams. As shown in a separate analysis [23], beam 2 was strongly affected by 1 and 4.4 Hz noise (see also the Appendix), which affected the data in the time interval used for the fit. Therefore, the difference in the numbers of data points between beam 1 and beam 2 comes from the detailed frequency analysis and resulted in a higher fraction of rejected samples for beam 2 than for beam 1.

Similarly, as in 2012 [8], the diffusion rates computed for inward steps are systematically larger than values obtained from the outward steps at the same transverse amplitude (see Fig. 11). Diffusion coefficients rates for a given beam or plane range from 3.6×10^{-11} to 1.2×10^{-8} μm^2/s. Compared to the diffusion rates that were found in 2012, which were in the range between 1.2×10^{-11} and 3.6×10^{-9} μm^2/s, we observe larger diffusion coefficients at 6.5 TeV. From the diffusion coefficient, one can also estimate the impact parameter, i.e., the depth at which particle touches the collimator. Although the detailed analysis goes beyond this paper, following estimates showed in previous work [26] leads to values of the impact parameter to be between 0.03 and 0.6 μm.

Apart from the main difference in energy (6.5 instead of 4 TeV), other important differences can be recalled.

Bunch spacing.—During the experiments in 2012 at 4 TeV, the LHC bunch spacing was 50 ns, hence with a reduced electron cloud effect [27]. The measurements at 6.5 TeV were performed with 25 ns spacing.

Beam brightness.—Beam brightness scales as $\sim \frac{N}{\sigma_x \sigma_y}$, where N is the number of bunches and $\sigma_{x,y}$ are the transverse beam sizes. During experiments at 6.5 TeV in LHC run 2, we operated with higher brightness than in LHC run 1.

Collimator settings.—With respect to the LHC design report and to the operation in LHC run 1 when the TCP half gap was opened as much as $7\sigma_N$ [28], the LHC run 2 settings were set tighter, at $5\sigma_N$ [9]. This increased the impedance seen by the beam.

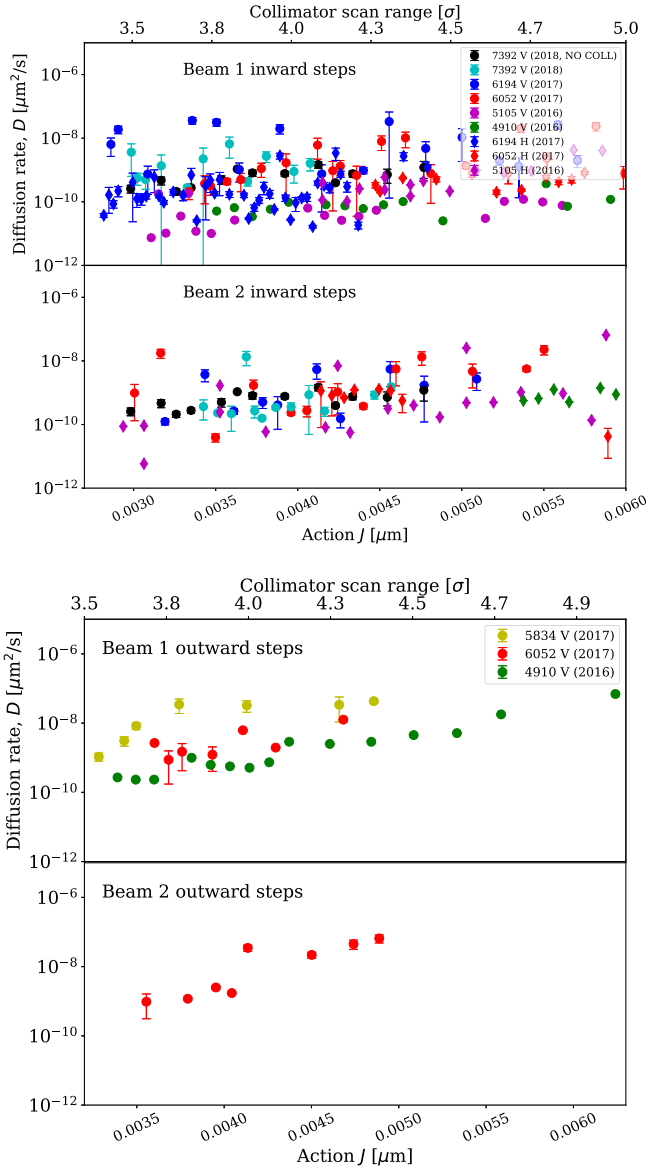

FIG. 11. Estimated diffusion coefficients for two beams for the inward (top) and the outward (bottom) steps. Different colors represent different fills from the summary in Table III. Each data point is an average of all bunch measurements from acquisitions at 100 Hz.

Emittance evolution.—During LHC run 2, there was emittance reduction due to radiation damping [29,30].

Optics.—During LHC run 2 (later part of 2017 and all of 2018), the beam optics was relying on the telescopic squeeze [14]. This optics features special chromatic properties and uses different integer tune values; optics variations in the arcs are used to reduce the β^* at the collision points, as opposed to the nominal LHC optics that relies only on local changes around the IPs to control β^* [1]. The modulation of the chromaticity in the arcs adjacent to the IPs provided the boost for the final squeeze but also changed the dynamics of the particles.

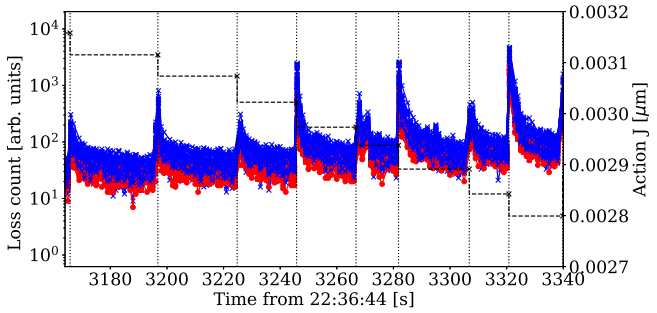

FIG. 12. Selected loss peaks resulting from the collimator steps. Data for beam 1 vertical scraping during fill 6052 with 2550b in 2017. The blue lines represent the bunches in the colliding trains while the red lines the 12 noncolliding bunches.

All this could be associated with the change of the diffusion coefficient, observed in measurements at 6.5 TeV. However, a detailed study of each of these effects goes beyond the scope of this paper. In any case, the observed diffusion coefficient values and their change with respect to the values measured in 2012 are still within the range of design requirements of the cleaning system [2].

C. Bunch-by-bunch diffusion coefficient

Figure 12 shows the overview of the scraping test done in fill 6052 as recorded by the dBLM detectors in acquisition mode 1. One can notice that the waiting times after different steps are not the same. This is related to the height of the loss spike. Every second spike is larger, and this is attributed to an overshoot of the position reached by the jaw. This alternating behavior for some jaws was identified by independent jaw-position measurements [6]. Lower-signal spikes correspond to the cases of smaller effective jaw steps. These were ignored in the analysis, and, correspondingly, the waiting time was shortened to speed the overall measurement, in favor of spikes with larger and cleaner signals.

For analysis purposes, we selected only a few steps that had clear and distinct loss peaks (fills 6052, 6194, and 7392), and we analyzed them from the bunch-by-bunch point of view. Recording losses with diamond detectors allowed us to separate the colliding bunches and non-colliding bunches (there is a train of 12 noncolliding bunches in each beam to probe beam-gas interactions) as well as to differentiate between colliding bunches at the beginning or at the end of the batch.

In some cases (using dBLM acquisition mode 1), the loss signal was integrated for similar bunches within trains (or all bunches within a train) to increase the overall signal resolution. Figure 13 shows the computed bunch-by-bunch diffusion coefficients for colliding and not colliding, showed along the full beam diffusion coefficient using the full model. Since the extracted diffusion coefficient depends mostly on the shape of the decay part, and not on

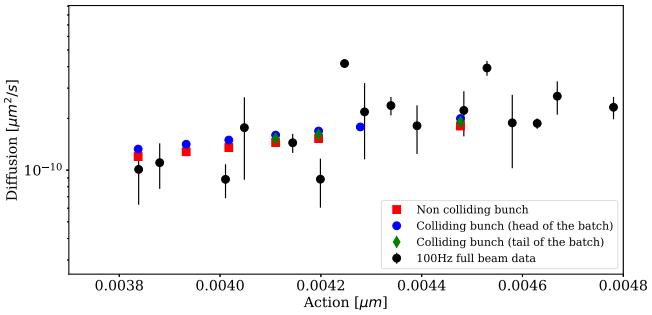

FIG. 13. Computed diffusion coefficient for different bunch families. Results obtained from dBLM acquisition mode 1 (in red, blue, and green) along IC-BLM (black), for fill 6052 (see Table III).

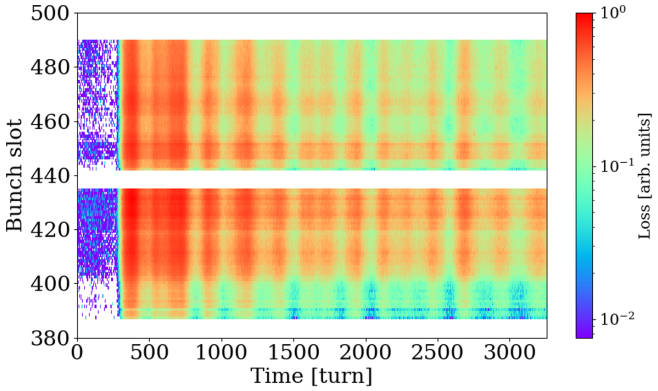

FIG. 15. Bunch-by-bunch losses recorded by dBLM acquisition mode 2 during one scan step in fill 7392 for beam 1 (details in Table III).

the absolute loss level, one can notice no correlation to the loss level seen in Fig. 12. For the arbitrarily chosen steps, beam diffusion coefficient was estimated from the dBLM acquisition mode 1 recordings along the filled rf buckets. Figure 14 shows the diffusion coefficient extracted, for the same steps as before, for the few first batches of the beam. There is no visible dependence of the diffusion coefficient on the position within the batches for fill 6052. At the same time, a decreasing trend along the scan is clearly noticeable.

The same analysis was performed for the case of turn-by-turn data using dBLM acquisition mode 2. With a properly triggered data acquisition, we recorded the moment when the collimator jaw step was performed. Figure 15 shows the bunch-by-bunch losses before the step (about 300 turns), during the step (another 500 turns), and after the collimator step (the remaining 2000 turns). For the same test case, bunch loss data along all 3000 turns and the result of the fitted model Eq. (2) were shown as an example in Fig. 6.

Figure 16 shows the results obtained from the turn-by-turn data collected for 96 bunches within two groups, and it reveals slight differences between the bunches even further. In that case, within the assumption that there are enough losses recorded to perform the analysis, one can see the increased uncertainty related to the level of the loss signal. This may be attributed to the different loss mechanisms, i.e., is related to the position in the batch and, therefore, to the different collision patterns and different number of long-range beam-beam (LRBB) encounters in the high-luminosity insertions (IR1 and IR5). For the same case, no clear correlation was found for the computed diffusion coefficient with the LRBB orbits shifts [31,32] nor with the different bunch collision classes (PACMAN [33]). This is not completely unexpected, as recent analyses of the typical lifetimes of the various bunches did not reveal any hint of a LRBB pattern during long periods without changes of the crossing angle or β^* [34]. Indeed, the value of the crossing angle ensures that the beam-beam is not the dominating source of beam losses, but rather the electron-cloud phenomena in the triplet quadrupoles [35]. This explains the experimental result reported here, as the measurement conditions were with only short trains, hence entailing low electron-cloud effects.

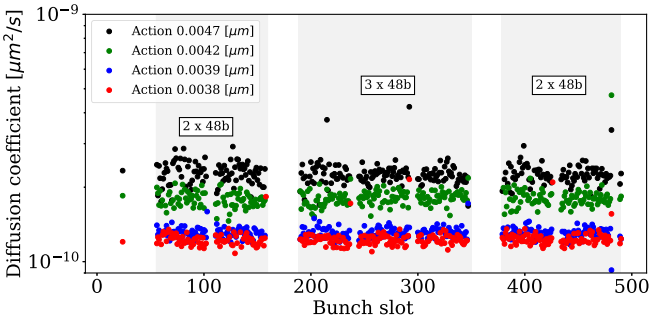

FIG. 14. Bunch-by-bunch diffusion coefficient obtained from dBLM acquisition mode 1 for fill 6052 (details in Table III). The four datasets belong to different steps and, therefore, different actions J. As it was an end-of-fill test, the bunch intensities were significantly lower than nominal.

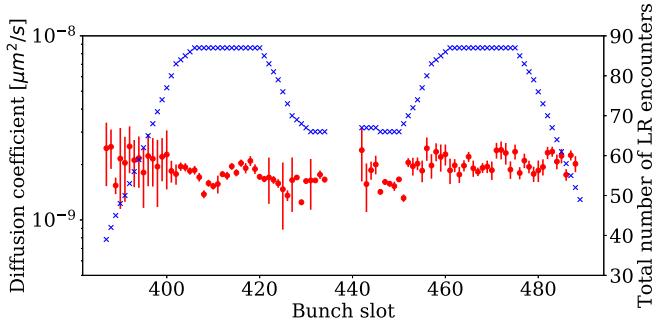

FIG. 16. In red, the diffusion coefficient for the different bunches computed from beam loss data (collected by dBLM acquisition mode 2), during one scan step (at $J_i = 0.0021$ μm and corresponding to the jaw position at 3.6σ) in fill 7392 for beam 1, is shown (details in Table III). In blue, the number of beam-beam long-range encounters per bunch slot is shown.

V. CONCLUSIONS AND OUTLOOK

Several measurement campaigns were performed between 2016 and 2018 to study the transverse halo repopulation mechanisms at the LHC at 6.5 TeV by means of proton beams used for physics, providing a first estimate of diffusion measurements at this energy. Collimator scans have been used to generate beam losses from which the halo population and the diffusion coefficient have been reconstructed at different transverse amplitudes. The experimental conditions cover a very broad range of configurations, which allowed measuring both colliding and noncolliding beams, horizontal and vertical effects, and low- and high-intensity beams. The values obtained for halo population and diffusion coefficients are, in general, larger than those measured in 2012 at 4 TeV. Although this level of beam losses was managed very well by the collimation system during LHC run 2, concern arises for the efficient operation of the HL-LHC, whenever the tail population reaches the level of several percent of the total beam intensity. However, this concern has been addressed through the implementation of active halo-control methods with hollow electron lenses, which have been recently integrated in the High-Luminosity LHC for a deployment in run 4 when upgraded beam parameters are planned. Furthermore, the observation of a significant tail overpopulation (with respect to a Gaussian distribution) for both high- and low-intensity beams needs to be taken into account for emittance reconstruction, even more importantly, for the future operation of HL-LHC.

Diamond beam loss monitors detectors were used for the first time to obtain the measurement of the diffusion coefficient of individual bunches, which is an essential result in view of scrutinizing the various phenomena that are affecting the several bunch in the LHC and HL-LHC. The outcome of the measurement campaign performed so far does not provide, for the specific machine configurations used in the measurements, any hint of beam-beam-related patterns in the values of the diffusion coefficient for individual bunches within colliding trains of bunches.

A good agreement between the results obtained with ionization chambers and diamond detectors has been found. The only drawback of the latter type of detectors is their rather small acceptance, which translates in a limited sensitivity at low loss levels. Except for the qualitative observations that halo diffusion is smaller for noncolliding bunches, the low beam losses recorded made it impossible using diamond detectors for measuring the diffusion coefficient, specifically for the 12 noncolliding bunches at the beginning of each beam.

It is worth mentioning that these devices opened up the possibility of short-timescale, turn-by-turn loss measurements covering a few hundred milliseconds. Therefore, in parallel with the main measurements and their analysis, other effects have been studied, such as the frequency spectrum of the measured beam losses. An outcome of these studies has been the identification of certain frequencies, which appear more distinct in the loss frequency spectra and might turn out useful in future analyses.

Finally, it is also worth mentioning that numerical and theoretical studies are currently carried out in order to devise possible improved experimental techniques to determine the value of the diffusion coefficient on the basis of measurements with collimator scans. In this respect, it is the goal to come to a definition of a novel experimental procedure to be tested during the forthcoming run 3 of the LHC.

ACKNOWLEDGMENTS

The authors thank the LHC machine coordinators and LHC Machine Development coordinators, for the possibility of conducting end-of-fill scans and for accommodating requests for beam time. Special thanks go to the LHC operation crew, who always actively helped with the experiments. One of the authors (M. G.) thanks G. Iadarola for useful discussions. The work of A. G. is supported by the HL-LHC Project. The authors thank the two anonymous referees for the excellent comments and suggestions. This manuscript has been authored by Fermi Research Alliance, LLC under Contract No. DE-AC02-07CH11359 with the U.S. Department of Energy, Office of Science, Office of High Energy Physics.

APPENDIX: FREQUENCY ANALYSIS OF LOSSES DURING COLLIMATOR SCANS

The availability of fast BLM acquisitions allows one to analyze the frequency content of losses at the collimators [26]. The availability of 100 Hz data improves the frequency range explored in previous measurements [6]. The prospect for frequency analyses is further extended by the availability of dBLM data. A Fourier analysis of the loss signals recorded during, or shortly after, the collimator steps was performed.

The 100 Hz data provide a continuous flow of measurements that enables analyses at each collimator step. An example is shown in Fig. 17, where, on top of a noisy signal, one can see dominating peaks around various frequencies (4, 10, 23, and 46 Hz). A similar analysis was performed for all the collimator steps during a complete scan, producing the "waterfall" plots in Fig. 18. The range up to 10 Hz is considered for comparison to previous analyses [6,8]. A peak at around 4.4 Hz was found for both beams. Peaks in this frequency range are not uncommon in accelerators [36] and can be attributed to various accelerator components, including the cryogenic system.

The same analysis can be applied to the dBLMs, showing the great potential of the new beam loss monitoring system [11]. The experiments discussed here induce high beam losses that are ideal for these measurements, as they ensure sufficiently high loss levels that can be recorded

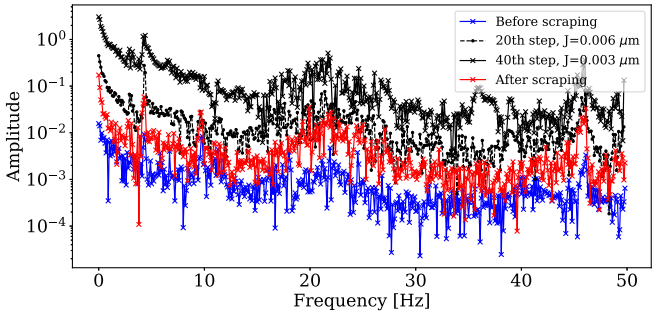

FIG. 17. Frequency analysis of the beam 1 vertical response for four moments. Before, during (in two steps), and after the scraping in fill 6052 (see Table III for details).

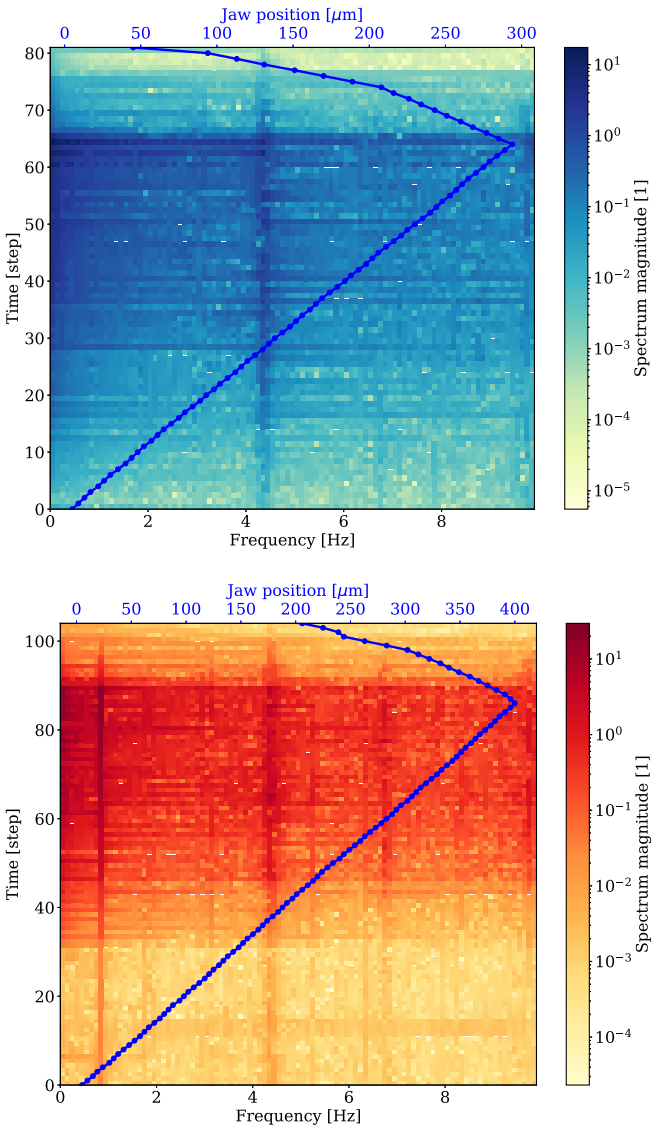

FIG. 18. Frequency analysis of the beam 1 vertical (top) and beam 2 vertical (bottom) response as a function of the steps (gap change). Distinct peaks around 1, 4.4, and 6.7 Hz can be seen. The blue line represents the moving jaw position as a function of the experiment step.

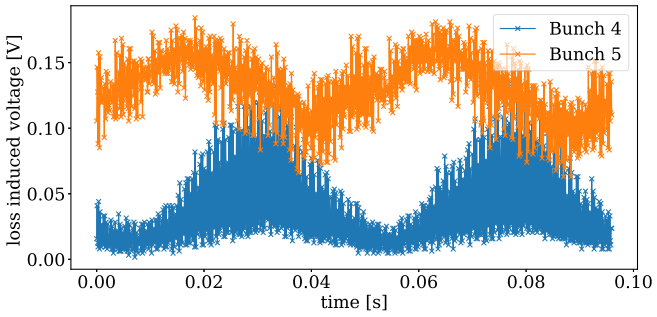

FIG. 19. dBLM acquisition mode 2 raw signal recorded for two arbitrarily selected bunches during one step performed in fill 6194 (see Table III for more details).

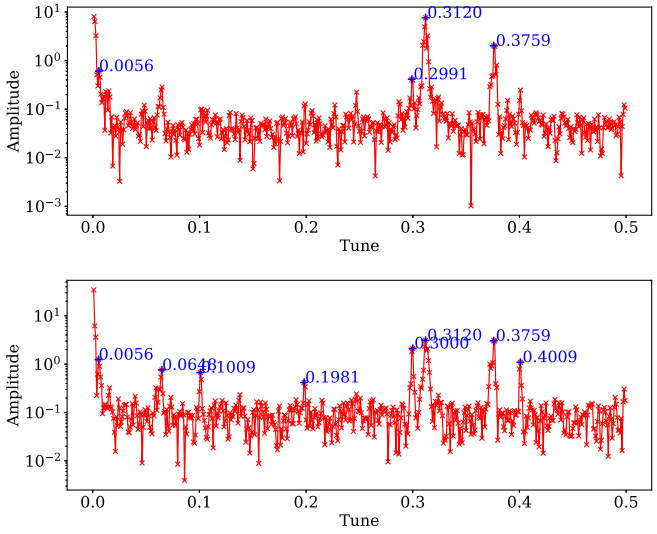

FIG. 20. Frequency analysis of the raw signal (Fig. 19) for bunch 4 (top) and bunch 5 (bottom) indicating local maxima in the region of the measured (BBQ) betatron tunes $Q_x = 0.30$ and $Q_y = 0.31$.

by the dBLM system (which are otherwise close to noise levels in standard operation). Specifically, the bunch-by-bunch loss signals can be measured reliably; see Fig. 19. A FFT analysis of these signals provides frequency spectra for each bunch (see some examples in Fig. 20), which can be used for indirect observation of the betatron tunes. The reconstructed values, although slightly off the nominal values (we did not correct the machine during the experiments), showed a good agreement with dedicated tune measurements, recorded with base band Q (BBQ) tune measurement [37]. These frequency spectra are shown here to illustrate the capabilities of the system. A detailed analysis is beyond the scope of this paper.

[1] M. Benedikt, P. Collier, V. Mertens, J. Poole, and K. Schindl, LHC design report, CERN, Geneva, 2004, https://cds.cern.ch/record/782076.

[2] R. W. Aßmann, J. B. Jeanneret, and D. I. Kaltchev, Status of robustness studies for the LHC collimation (to be published), https://www.researchgate.net/publication/239531383_STATUS_OF_ROBUSTNESS_STUDIES_FOR_THE_LHC_COLLIMATION.
[3] K.-H. Mess and M. Seidel, Collimators as diagnostic tools in the proton machine of HERA, Nucl. Instrum. Methods Phys. Res., Sect. A **351**, 279 (1994).
[4] G. Apollinari, I. B. Alonso, O. Brüning, M. Lamont, and L. Rossi, High-Luminosity Large Hadron Collider (HL-LHC): Preliminary design report, CERN Yellow Reports: Monographs, CERN, Geneva, 2015, https://cds.cern.ch/record/2116337.
[5] LHC Injector Upgrade Project, https://espace.cern.ch/liu-project/default.aspx.
[6] G. Valentino, R. Bruce, A. Gorzawski, S. Redaelli, G. Trad, J. Wagner, and C. Xu, End-of-fill diffusion and halo population measurements with physics beams at 6.5 TeV, CERN Technical Report No. CERN-ACC-NOTE-2017-0049, 2017.
[7] G. Valentino, R. Assmann, R. Bruce, F. Burkart, S. Redaelli, B. Salvachua, V. Previtali, G. Stancari, and A. Valishev, Halo scraping, diffusion and repopulation MD, Technical Report No. CERN-ATS-Note-2012-074 MD, 2012.
[8] G. Valentino, R. Aßmann, R. Bruce, F. Burkart, V. Previtali, S. Redaelli, B. Salvachua, G. Stancari, and A. Valishev, Beam diffusion measurements using collimator scans in the LHC, Phys. Rev. Accel. Beams **16**, 021003 (2013).
[9] J. Wenninger, Operation and configuration of the LHC in run 2, Technical Report No. CERN-ACC-NOTE-2019-0007, 2019.
[10] G. Stancari, G. Annala, T. Johnson, D. Still, and A. Valishev, Measurements of transverse beam diffusion rates in the Fermilab Tevatron Collider, in *Proceedings of the 2nd International Particle Accelerator Conference, San Sebastián, Spain* (EPS-AG, Spain, 2011), TUPZ033, pp. 1882–1884.
[11] A. Gorzawski, S. Redaelli, N. F. Martinez, H. G. Morales, A. Mereghetti, C. Xu, G. Valentino, and R. B. Appleby, Fast loss analysis with LHC diamond detectors in 2017, Technical Report No. CERN-ACC-NOTE-2018-0041, 2018.
[12] G. Stancari, Diffusion model for the time evolution of particle loss rates in collimator scans: A method for measuring stochastic transverse beam dynamics in circular accelerators, arXiv:1108.5010.
[13] G. Valentino, R. Aßmann, R. Bruce, S. Redaelli, A. Rossi, N. Sammut, and D. Wollmann, Semiautomatic beam-based LHC collimator alignment, Phys. Rev. Accel. Beams **15**, 051002 (2012).
[14] S. Fartoukh, Achromatic telescopic squeezing scheme and application to the LHC and its luminosity upgrade, Phys. Rev. Accel. Beams **16**, 111002 (2013).
[15] F. S. Carlier, J. M. C. De Portugal Martinez Vazquez, S. Fartoukh, E. Fol, D. Gamba, A. G.-T. Valdivieso, M. Giovannozzi, M. Hofer, A. S. Langner, E. H. Maclean, L. Malina, L. M. M. Medrano, T. H. B. Persson, P. K. Skowronski, R. T. Garcia, F. Van Der Veken, and A. Wegscheider, Optics measurements and correction challenges for the HL-LHC, Technical Report No. CERN-ACC-2017-0088, CERN, Geneva, 2017.
[16] B. Dehning, Beam loss monitors at LHC, CERN Yellow Rep.: Monogr. **2**, 303 (2016).
[17] C. Zamantzas, B. Defining, E. Effinger, J. Emery, G. Ferioli, and S. Jackson, The LHC beam loss monitoring system's data contribution to other systems, in *Proceedings of IEEE Nuclear Science Symposium Conference Record, Honolulu, HI, 2007*, pp. 2331–2335, http://www.proceedings.com/02681.html.
[18] E. Griesmayer and B. Dehning, Diamonds for beam instrumentation, Phys. Procedia **37**, 1997 (2012).
[19] G. Trad, G. Baud, E. Bravin, B. Dehning, M. Ferroluzzi, A. Goldblatt, E. Piselli, F. Roncarolo, J. Storey, and Q. Veyrat, Status of the beam profile measurements at the LHC, in *Proceedings of the 6th Evian workshop on LHC beam operation, Evian Les Bains, France, 2015* (CERN, Geneva, 2016), pp. 163–170.
[20] C. Roderick, R. Billen, R. D. G. Aparicio, E. Grancher, A. Khodabandeh, and N. S. Chinchilla, The LHC logging service: Handling terabytes of on-line data, Technical Report No. CERN-ATS-2009-099, CERN, Geneva, 2009.
[21] B. Efron and R. J. Tibshirani, *An Introduction to the Bootstrap* (Springer, Boston, 1993).
[22] A. C. Davison and D. V. Hinkley, *Bootstrap Methods and Their Application* (Cambridge University Press, Cambridge, England, 1997).
[23] A. Gorzawski, Halo cleaning: What have we learned from 2017, in *Proceedings of the 7th HL-LHC Collaboration Meeting, Madrid, Spain, 2017*, https://indico.cern.ch/event/647714/.
[24] B. Salvachua, R. W. Assmann, R. Bruce, F. Burkart, S. Redaelli, G. Valentino, and D. Wollmann, Lifetime analysis at high intensity colliders applied to the LHC, Technical Report No. CERN-ACC-2013-0072, 2013.
[25] HL-LHC baseline parameters, https://espace.cern.ch/HiLumi/WP2/Wiki/HL–LHC%20Parameters.asp.
[26] M. Seidel, The proton collimation system of HERA, Ph.D. thesis, Hamburg University, 1994.
[27] G. Iadarola, G. Rumolo, P. Dijkstal, and L. Mether, Analysis of the beam induced heat loads on the LHC arc beam screens during run 2, Technical Report No. CERN-ACC-NOTE-2017-0066, 2017.
[28] R. Alemany-Fernandez, E. Bravin, L. Drosdal, A. Gorzawski, V. Kain, M. Lamont, A. Macpherson, G. Papotti, M. Pojer, L. Ponce, S. Redaelli, G. Roy, M. S. Camillocci, W. Venturini, and J. Wenninger, Operation and configuration of the LHC in run 1, Technical Report No. CERN-ACC-NOTE-2013-0041, 2013.
[29] M. Hostettler, Luminosity evolution and optimum fill length, technical report, CERN LHC operation meeting, CERN, Geneva, 2016, https://indico.cern.ch/event/546248/contributions/2216246/attachments/1298096/1936445/LumiLifetime_LMC062016_v2.pdf.
[30] M. Hostettler, Emittance evolution in the LHC, in *Proceedings of the 8th LHC operation workshop, Geneva, 2019*, edited by T. Argyropoulos, S. Dubourg, and G. Trad, pp. 157–160, https://indico.cern.ch/event/663598/timetable/#20171212.detailed.

[31] A. A. Gorzawski, K. Fuchsberger, M. Hostettler, T. Pieloni, and J. Wenninger, Long-range beam-beam orbit effects in LHC, simulations and observations from machine operation in 2016, in *Proceedings of the International Particle Accelerator Conference (IPAC'17), Copenhagen, Denmark, 2017*, International Particle Accelerator Conference No. 8 (JACoW, Geneva, 2017), pp. 3799–3802, https://doi.org/10.18429/JACoW-IPAC2017-THPAB042.

[32] M. Hostettler, K. Fuchsberger, G. Papotti, Y. Papaphilippou, and T. Pieloni, Luminosity scans for beam diagnostics, Phys. Rev. Accel. Beams **21**, 102801 (2018).

[33] W. Herr, Effects of PACMAN bunches in the LHC, Technical Report No. LHC-Project-Report-39 (CERN, Geneva, 1996).

[34] G. Iadarola, Beam lifetime in collision—LHC experience, in *Proceedings of the 160th HiLumi WP2 Meeting, 2020* (to be published), https://indico.cern.ch/event/850136/contributions/3572984/.

[35] G. Iadarola (private communication).

[36] G. Stancari, New methods of particle collimation in colliders, arXiv:1110.0144.

[37] M. Gasior and R. Jones, High sensitivity tune measurement by direct diode detection, Technical Report No. CERN-AB-2005-060, 2005.